From telescope to computed tomography via sparse recovery approaches

Chao Wang

TETRAPODS Institute of Data Science
University of California, Davis

MADDD Seminar (Oct. 13, 2020)

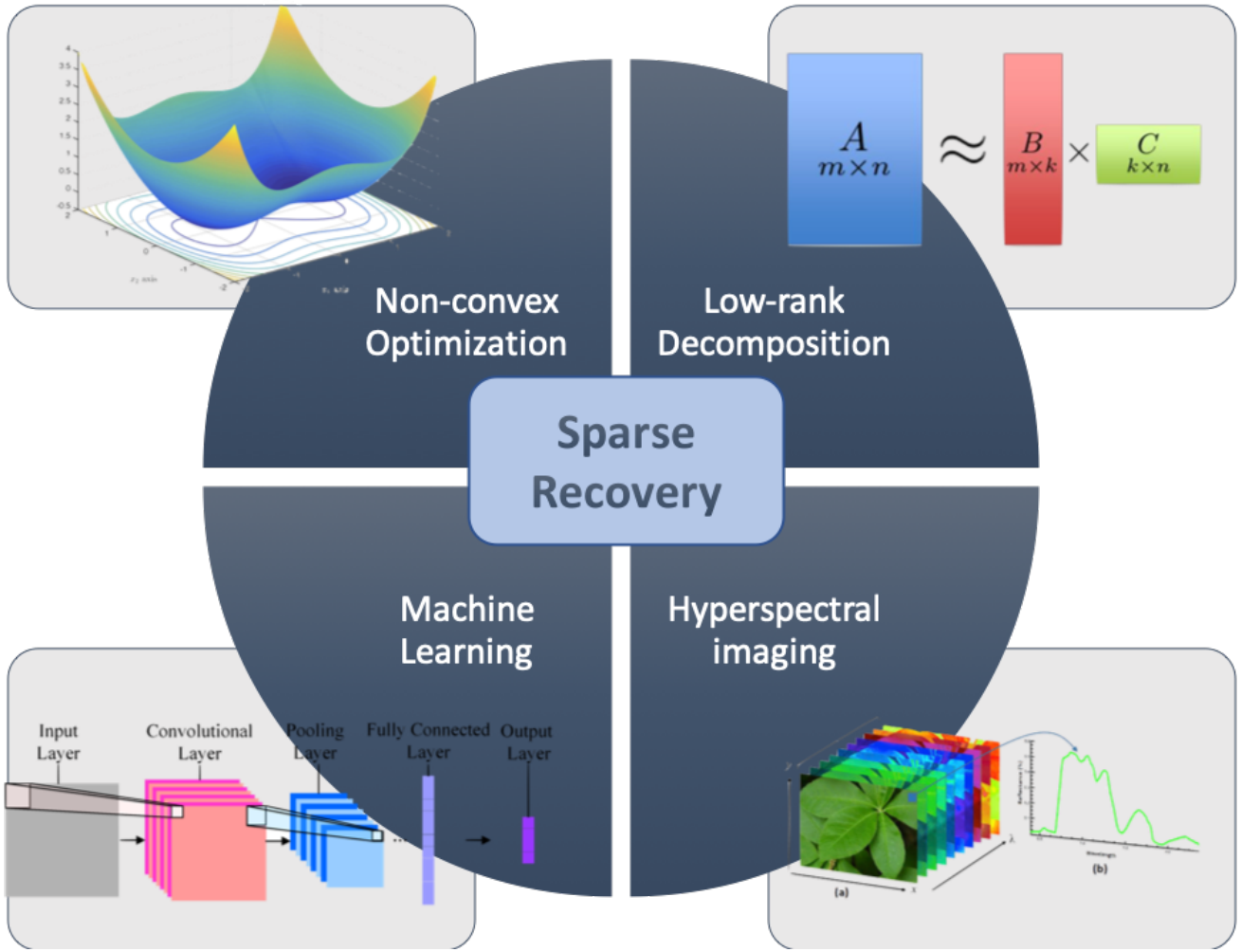
Non-convex Optimization
Low-rank Decomposition
Sparse Recovery
Machine Learning
Hyperspectral imaging
$A_{m\times n} \approx B_{m\times k} \times C_{k\times n}$
Input Layer
Convolutional Layer
Pooling Layer
Fully Connected Layer
Output Layer

Overview

1. PSF engineering and 3D imaging
   - Background
   - Problem Statement
   - Optimization scheme
2. Limited-angle CT reconstruction
   - L_1/L_2 on signal processing
   - L_1/L_2 on image processing
3. Conclusions

Point Spread Function Engineering and 3D Imaging

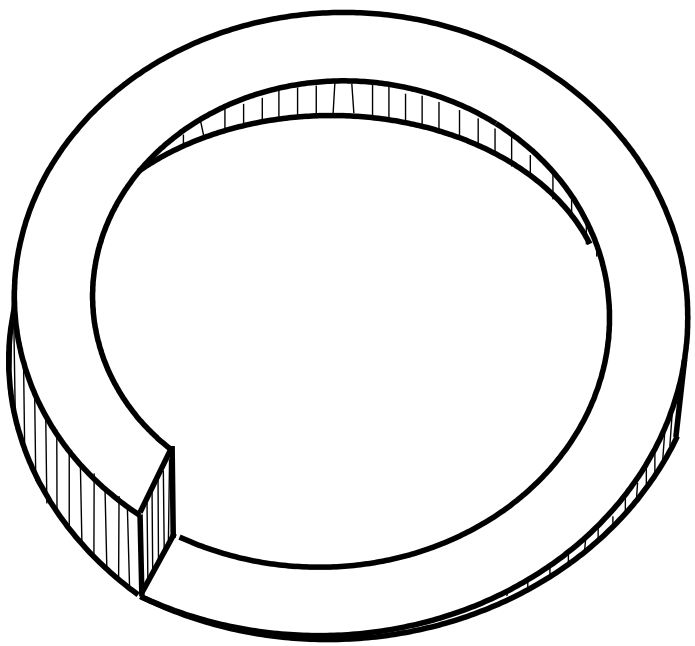

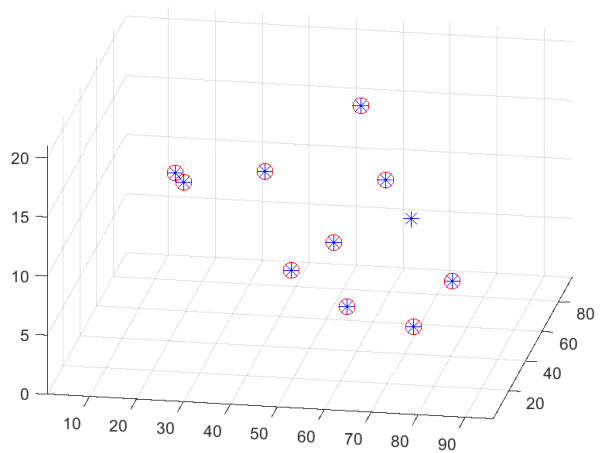

2D into 3D (Depth from focus)

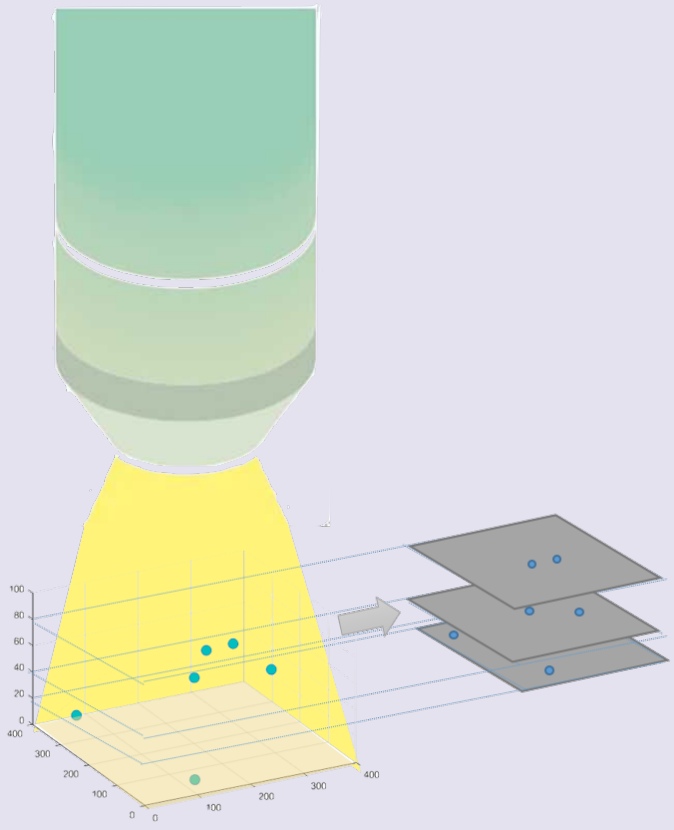

3D localization by scanning sequence of 2D images

computer

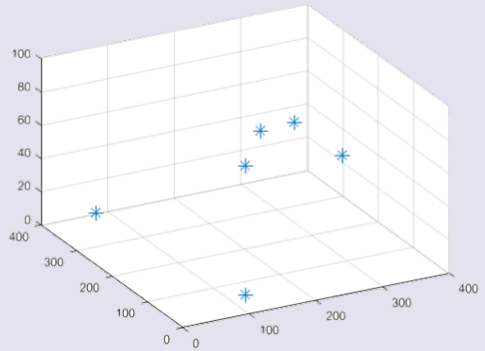

2D into 3D (Depth from defocus)

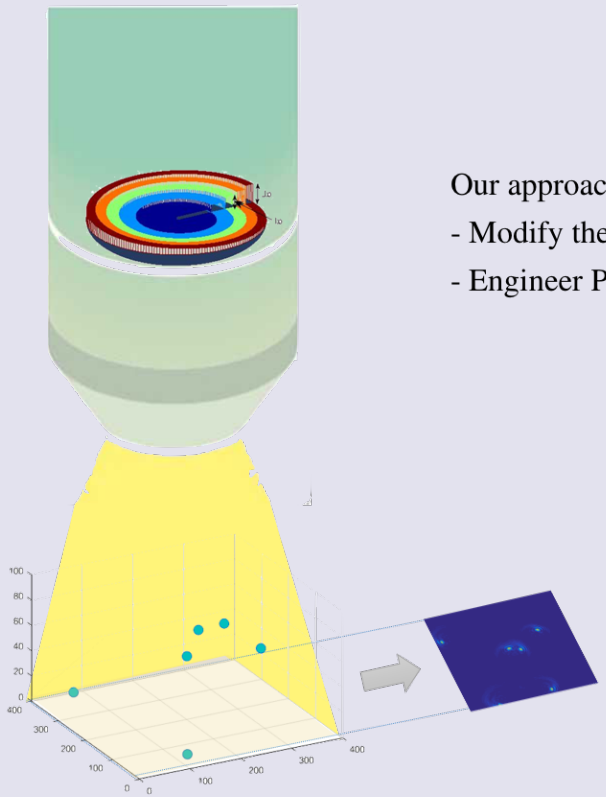

Our approach:

- Modify the camera optical system
- Engineer PSF to obtain 3D info from ONE 2D snapshot

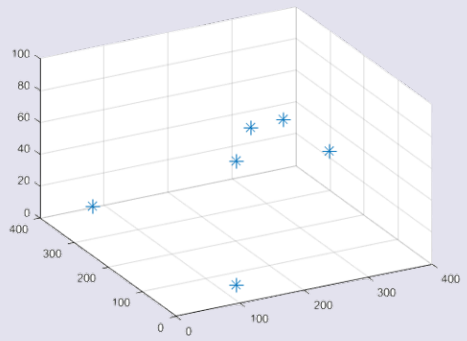

Background

Space safety problem: detecting and quantifying space junk

Credit to [www.extremetech.com]

Microscopy problem: obtaining 3D structures of live cells by single molecule localization

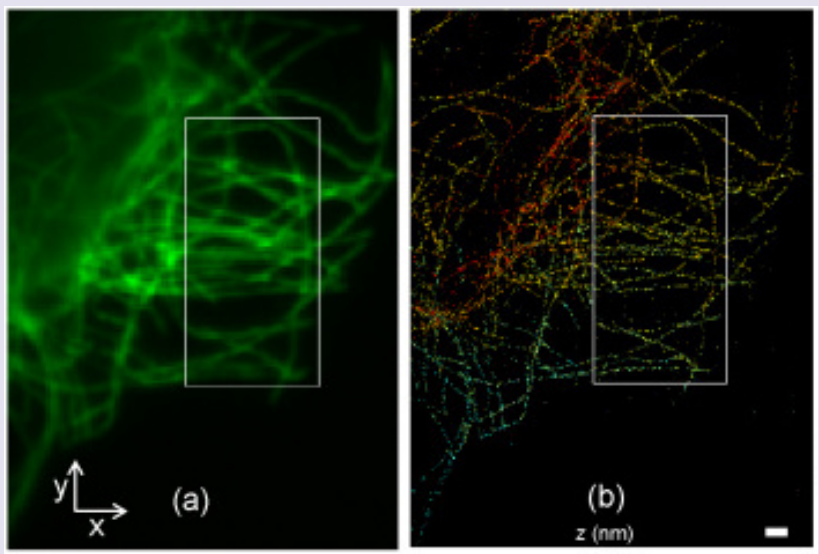

Credit to [G. Grover et al. 2012]

Telescope System for Space Debris Localization

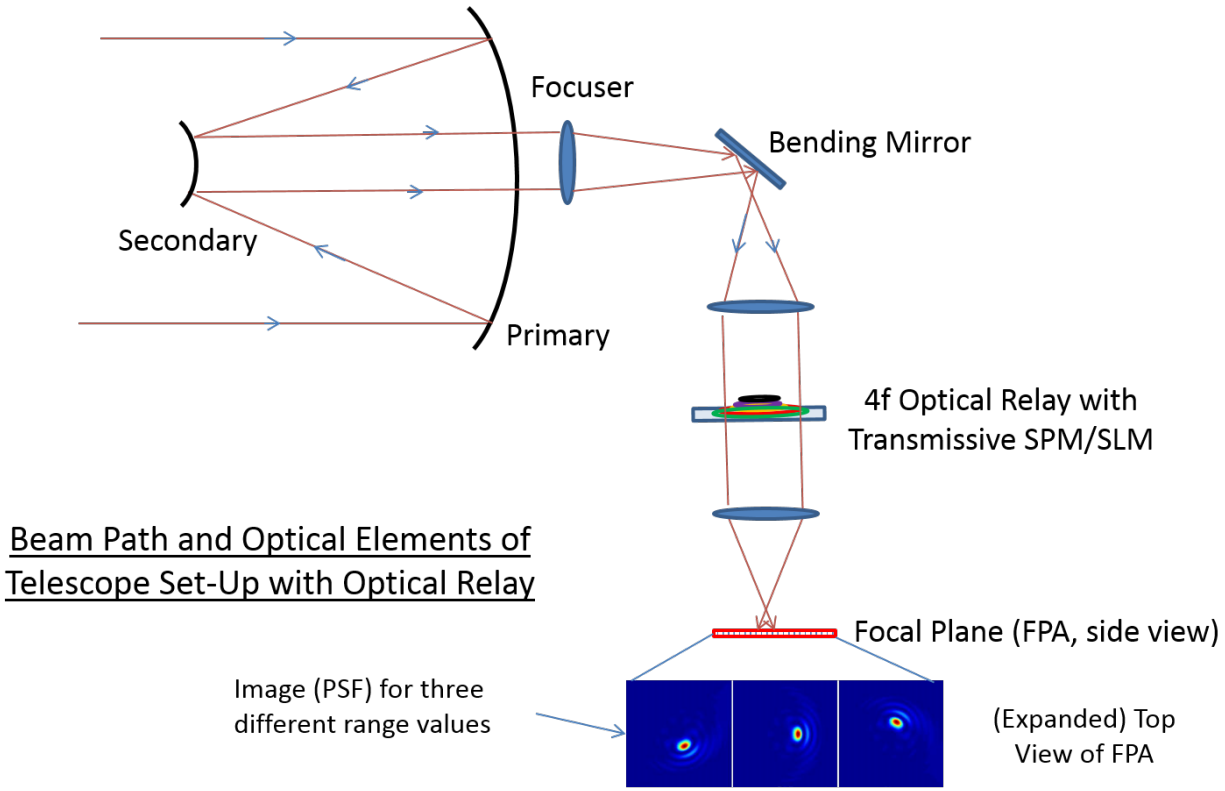

- Proposed in [Prasad 2013]
- Space based system for tracking debris - funded by US AFOSR

Conventional PSFs when imaging a point source

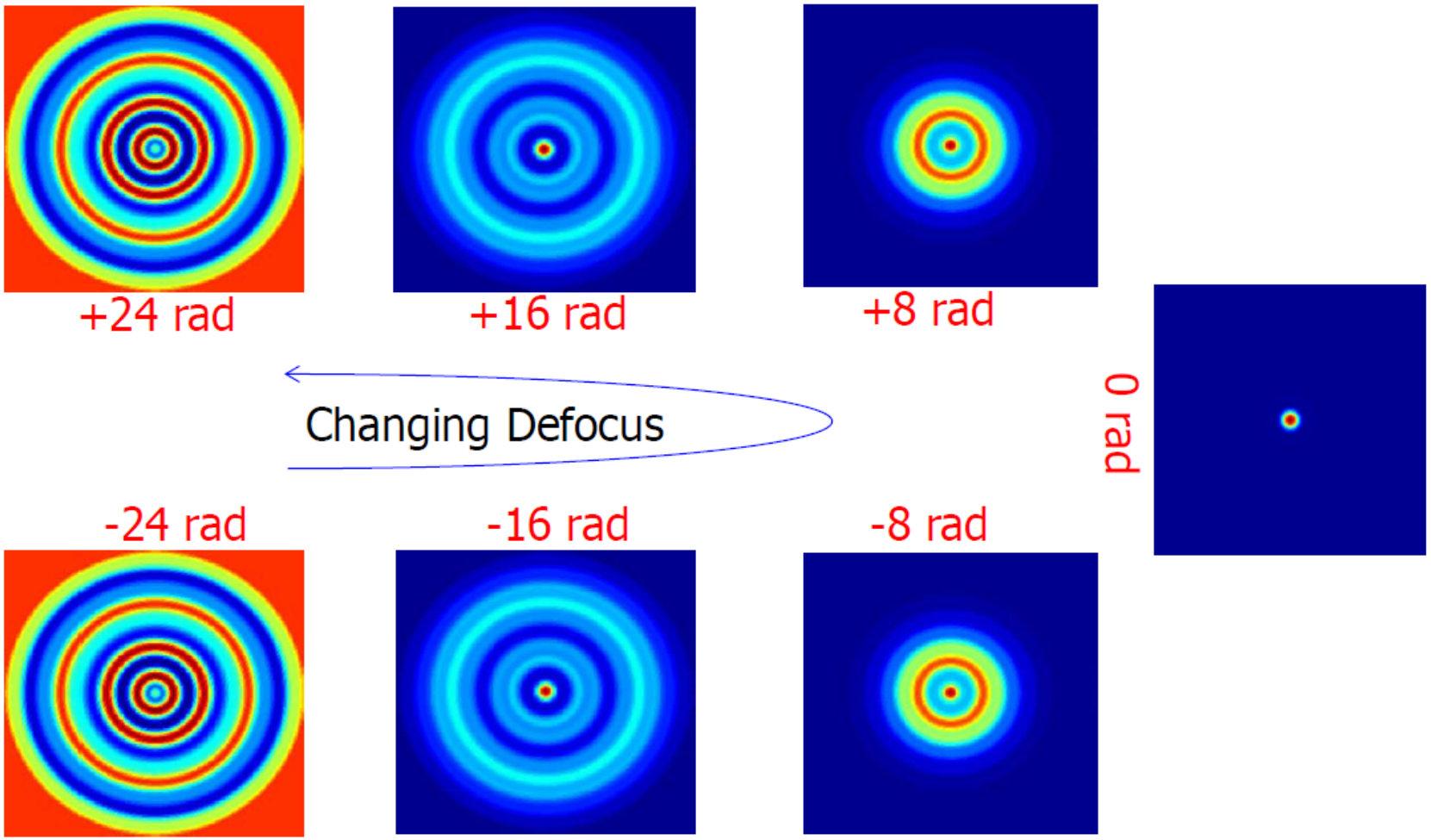

- Excellent in-focus 2D resolution (Rayleigh limit)
- High blur with increasing defocus – terrible 3D resolution/sensitivity!

Single Lobe (SL) point source images using engineered spiral phase mask

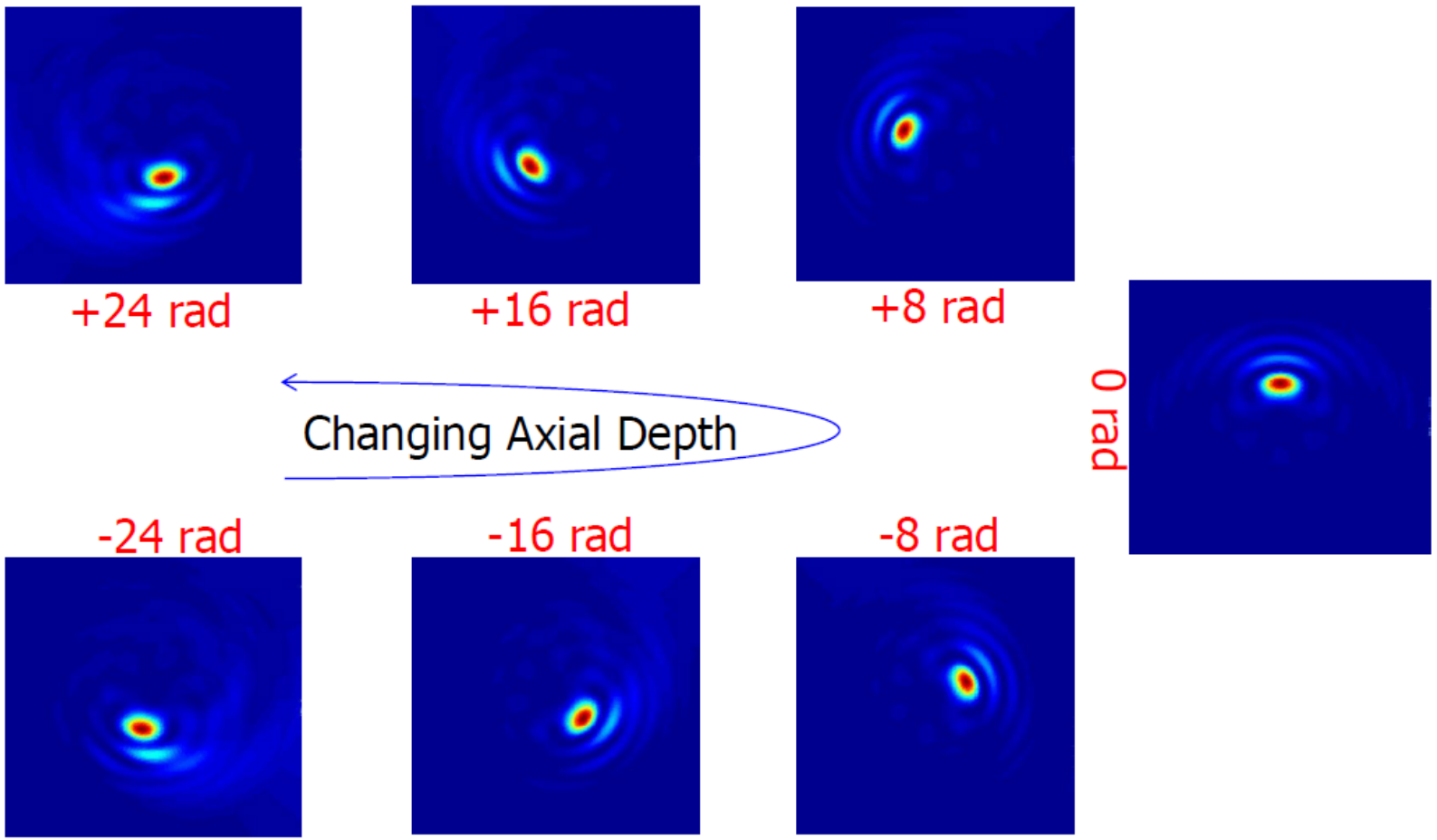

- One full rotation over Δ (defocus) = $2M\pi$ radians (DOF ~ $\pm$ M λ/NA^2)
- Single-lobe PSF with relatively stable shape/size
- High 3D image capture/reconstruction sensitivity even at low-light levels

Phase masks other than SL can enable PSF rotation

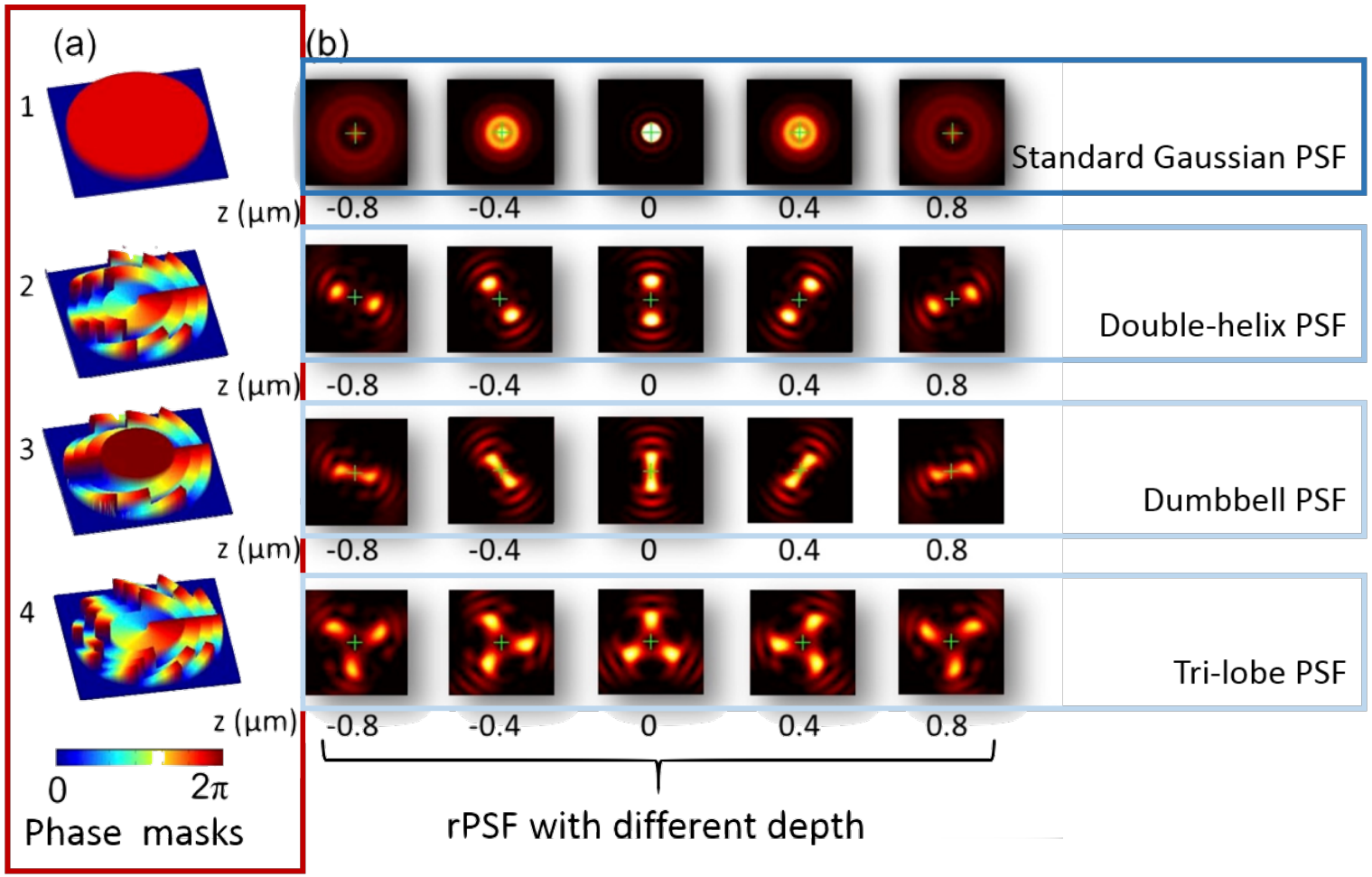

Credit to [Shuang, ..., Landes 2016]

Figure: (a): Some other kinds of phase masks & rotating PSFs, (b): images correspond to one point source in different depth positions.

Physics Model of SL Rotating PSF

- **Fourier Optics Formula for rPSF**

$$A_\zeta(\mathbf{s}) = \frac{1}{\pi}\left|\int P(\mathbf{u})\exp\left[\iota(2\pi\mathbf{u}\cdot\mathbf{s}+\zeta u^2-\psi(\mathbf{u}))\right]d\mathbf{u}\right|^2$$

- **Defocus parameter:**

$$\zeta = -\frac{\pi\delta z R^2}{\lambda l_0(l_0+\delta z)},$$

- $\psi(\mathrm{s}) = l\phi_\mathrm{s}$ when $\sqrt{(l-1)/L} \le s \le \sqrt{l/L},\ l = 1,\cdots,L$
- P is a pupil function and $\iota = \sqrt{-1}$.
- (s, ϕ_s) is the polar coordinate of normalized position.

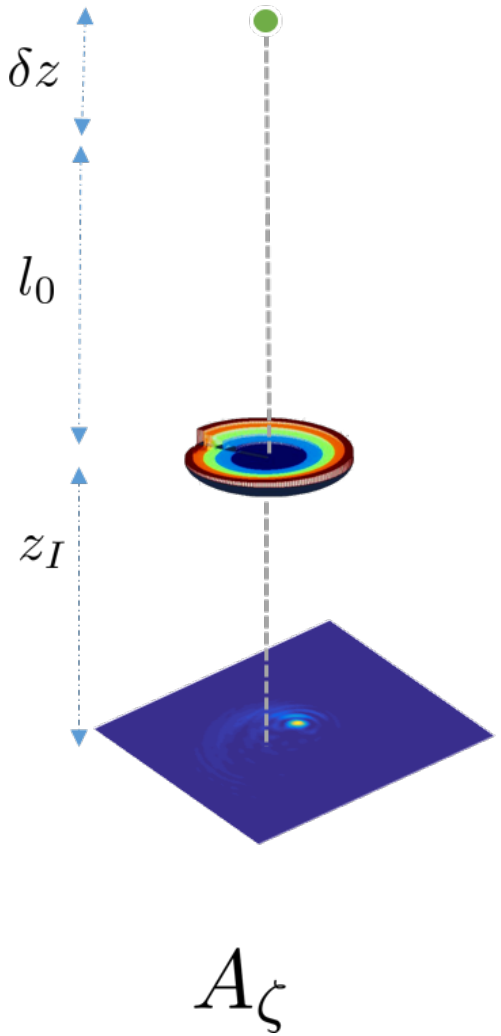

Physics Model of SL Rotating PSF

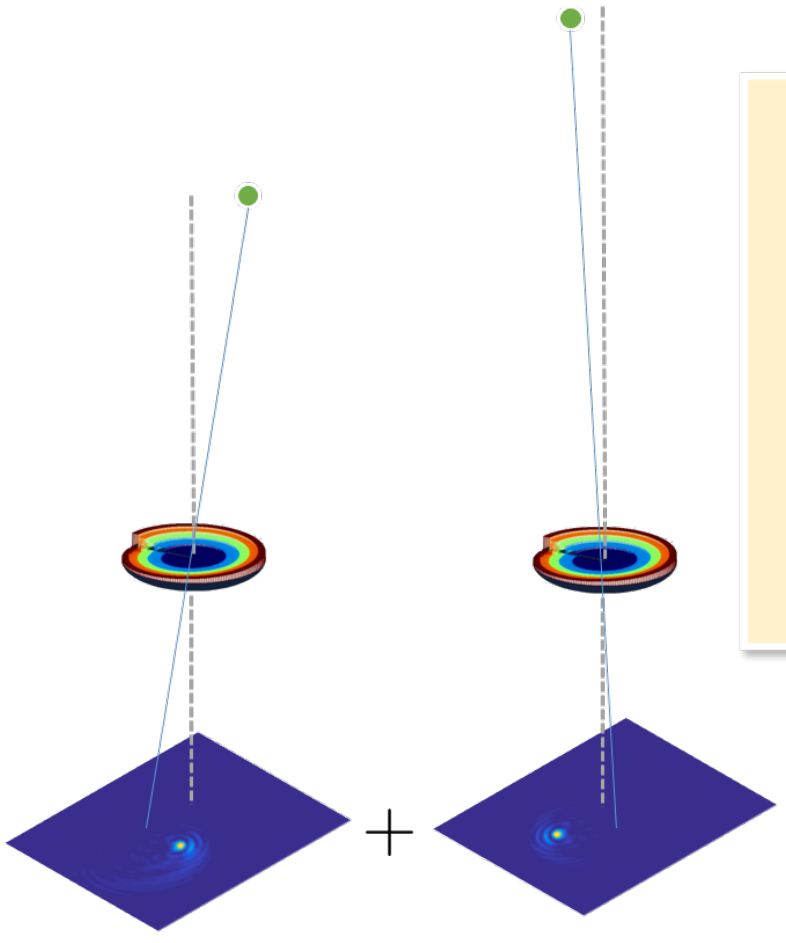

$f_1 \cdot (A_{\zeta_1} * \delta(x_1, y_1))$ $f_2 \cdot (A_{\zeta_2} * \delta(x_2, y_2))$

- The observed 2D image

$$\sum_{i=1}^{P} f_i \cdot (A_{\zeta_i} * \delta(x_i, y_i)) + N$$

- N is noise, P is the number of point sources,
- $(\delta(x,y))_{uv} = \begin{cases} 1, & (u,v) = (x,y) \\ 0, & \text{other} \end{cases}$
- 3D information: $(-\frac{z_I x_i}{l_0+\delta z_i}, -\frac{z_I y_i}{l_0+\delta z_i}, l_0 + \delta z_i)$

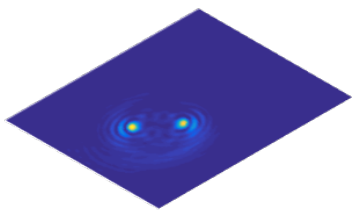

$\sum_{i=1}^{2} f_i \cdot (A_{\zeta_i} * \delta(x_i, y_i))$

Discretization

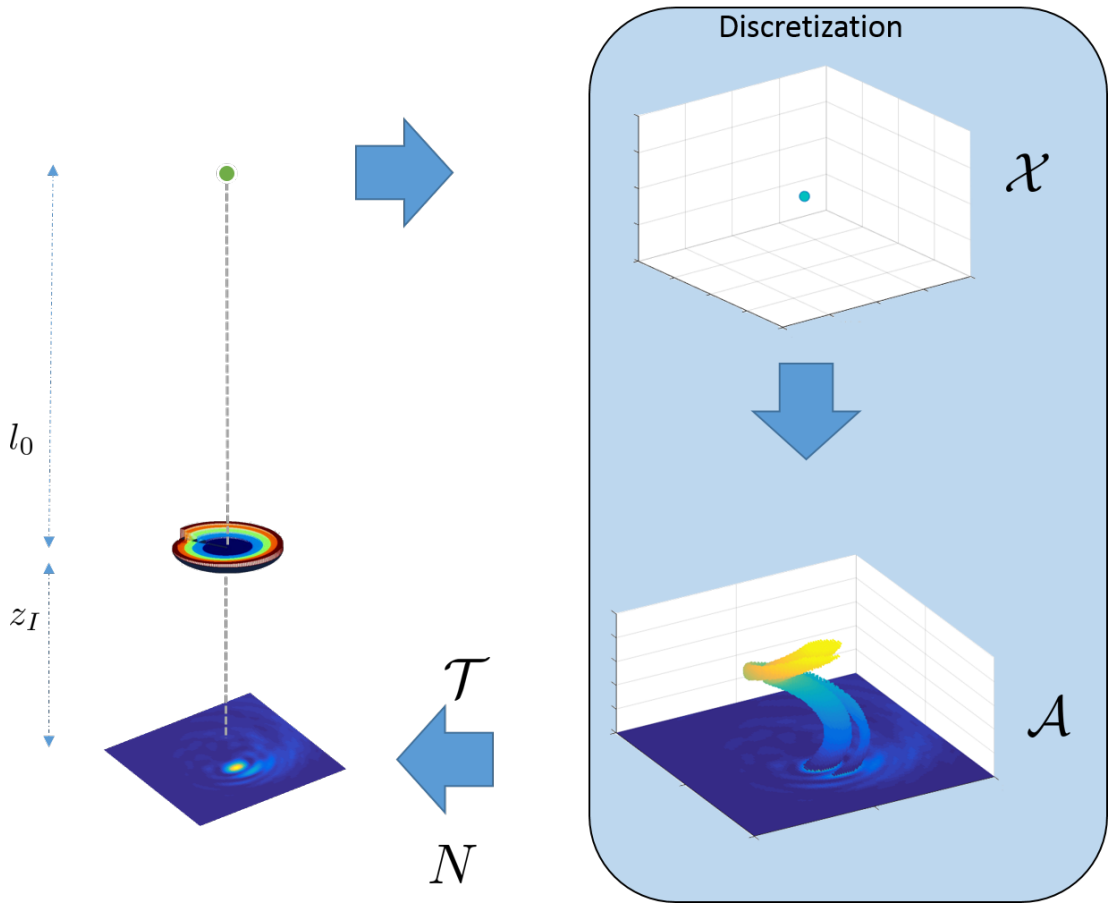

- Order the slices of $\mathcal{A}$ such that the last slice is corresponding to rPSF when $x, y, \delta z = 0$.
- We need to do 3D convolution $\mathcal{A} * \mathcal{X}$ when x, y or $\delta z \neq 0$,

Forward model with 2 point sources

forward model

The 2D observed image $G \in \mathbb{R}^{m \times n}$ can be represented as

$$G = N(\mathcal{T}(\mathcal{A} * \mathcal{X}))$$

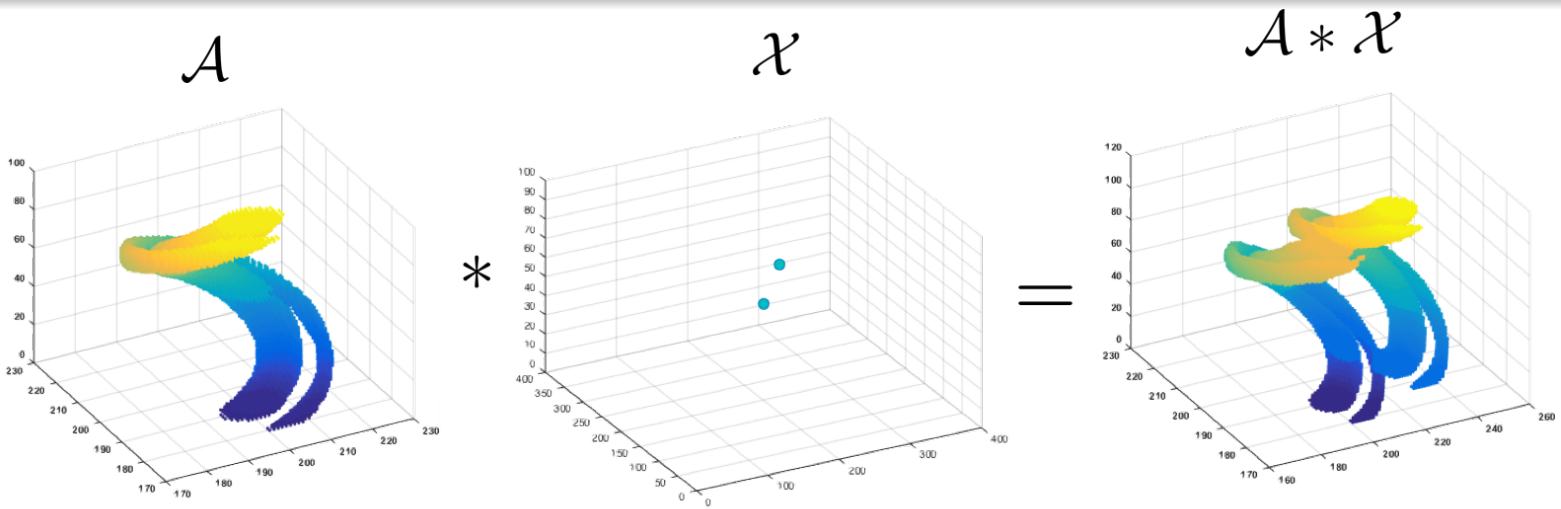

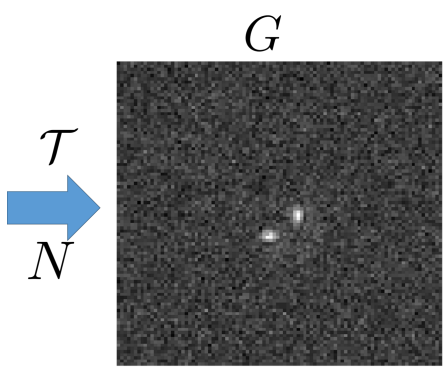

Optimization Problem

l_0 model

$$\begin{aligned} \min_{\mathcal{X}} \quad & \|\mathcal{X}\|_0 \\ \text{s.t.} \quad & \mathcal{D}(\mathcal{T}(\mathcal{A} * \mathcal{X})) < \epsilon, \end{aligned}$$

- To find the locations and values the the true point sources is a sparse recovery problem.
- Gaussian noise case
  - ℓ_0 model:

$$\begin{aligned} \min_{\mathcal{X}} \quad & \|\mathcal{X}\|_0 \\ \text{s.t.} \quad & \|\mathcal{T}(\mathcal{A} * \mathcal{X}) + b1 - G\|_F < \epsilon, \end{aligned}$$

  - ℓ_0 regularization model:

$$\min_{\mathcal{X}} \ \frac{1}{2} \|\mathcal{T}(\mathcal{A} * \mathcal{X}) + b1 - G\|_F^2 + \mu \|\mathcal{X}\|_0.$$

Gaussian noise case

Continuous Exact ℓ_0 algorithm (CEL0) applied on rPSF:

$$\min_{\mathcal{X}} \ \frac{1}{2}\|\mathcal{T}(\mathcal{A} * \mathcal{X}) - G\|_F^2 + \Phi_{\mathrm{CEL0}}(\mathcal{X}).$$

where

$$\Phi_{\mathrm{CEL0}}(\mathcal{X}) = \sum_{i=1}^{P} \phi(\|a_i\|, \lambda, ; \mathcal{X}),$$

$$\phi(a, \lambda, ; u) = \lambda - \frac{a^2}{2}\left(|u| - \frac{\sqrt{2\lambda}}{a}\right)^2 \mathbb{1}_{\{|u| \le \frac{\sqrt{2\lambda}}{a}\}},$$

$$\mathbb{1}_{\{u \in E\}} = \begin{cases} 1 & \text{if } u \in E; \\ 0 & \text{others.} \end{cases}$$

- Global minimizers of ℓ_0 model are contained in the global minimizers of CEL0;
- A transformation on a minimizer of CEL0 model will get a minimizer of ℓ_0 model;
- CEL0 can avoid some local minimizers of ℓ_0 model.

C. Wang, *et al.* IPIP 2018 (Springer).

Poisson Noise Case

Data Fitting Term

- Gaussian noise model:

$$\frac{1}{2}\|\mathcal{T}(\mathcal{A} * \mathcal{X}) + b1 - G\|_F^2$$

$$\Downarrow$$

- Poisson noise model:

$$D_{KL}(\mathcal{T}(\mathcal{A} * \mathcal{X}) + b1, G),$$

- The uniform background is denoted by b and 1 is a matrix with all entries 1.
- $D_{KL}(\mathcal{T}(\mathcal{A} * \mathcal{X}) + b1, G)$ can be rewritten as

$$\langle 1, \mathcal{T}(\mathcal{A} * \mathcal{X}) G \log(\mathcal{T}(\mathcal{A} * \mathcal{X}) + b1)\rangle.$$

Poisson Noise Model Optimization Problem

Optimization Problem

$$\min_{\mathcal{X}\geq 0} D_{KL}(\mathcal{T}(\mathcal{A} * \mathcal{X}) + b1, G) + \mu\mathcal{R}(\mathcal{X}).$$

- We choose $\mathcal{R}(\mathcal{X})$ to be a nonconvex and nondifferentiable function

$$\mathcal{R}(\mathcal{X}) := \sum_{i,j,k=1}^{m,n,d} \frac{|\mathcal{X}_{ijk}|}{a + |\mathcal{X}_{ijk}|},$$

where the tensor $\mathcal{X}$ is $m \times n \times d$ and a **is fixed and determines the degree of nonconvexity**.

Minimization Problem: KL-NC

The minimization problem (KL-NC) is

$$\min_{\mathcal{X}\geq 0} \left\{ \langle 1, \mathcal{T}(\mathcal{A} * \mathcal{X}) - G \ln(\mathcal{T}(\mathcal{A} * \mathcal{X}) + b\,1)\rangle + \mu \sum_{i,j,k=1}^{m,n,d} \frac{|\mathcal{X}_{ijk}|}{a + |\mathcal{X}_{ijk}|} \right\}.$$

Iteratively reweighted ℓ_1 algorithm (IRL1)

$$\begin{cases} w_{ijk}^{l} & = \frac{a\mu}{\left(a+\hat{\mathcal{X}}_{ijk}^{l}\right)^2}, \quad \forall i,j,k \\ \hat{\mathcal{X}}^{l+1} & = \arg\min_{\mathcal{X}\geq 0} \left\{ \langle 1,\ \mathcal{T}(\mathcal{A} * \mathcal{X}) - G \log(\mathcal{T}(\mathcal{A} * \mathcal{X}) + b\,1)\rangle + \sum_{i,j,k=1}^{m,n,d} w_{ijk}^{l} |\mathcal{X}_{ijk}| \right\} \end{cases}$$

Post-processing: Removing False Positive

- Computing the centroid of clustered point sources

$$x = \frac{\sum_{(i,j,k)\in C} i\mathcal{X}_{ijk}}{\sum_{(i,j,k)\in C} \mathcal{X}_{ijk}}; \quad y = \frac{\sum_{(i,j,k)\in C} j\mathcal{X}_{ijk}}{\sum_{(i,j,k)\in C} \mathcal{X}_{ijk}}; \quad z = \frac{\sum_{(i,j,k)\in C} k\mathcal{X}_{ijk}}{\sum_{(i,j,k)\in C} \mathcal{X}_{ijk}}.$$

- Searching neighbor from the brightest point source
- Setting a tolerant distance that for distinguishing one point source

Fixed Point Iterative Scheme for Estimating the Flux

- Based on data fitting term: $\nabla D_{KL}(H\mathbf{f} + b\mathbf{1}, \mathbf{g}) = 0$

Fixed Point Iterative Scheme

$$\mathbf{f}^{n+1} = \mathbf{f}_G + \mathcal{K}(\mathbf{f}^n), \quad n = 1, 2, \cdots \tag{1}$$

where

$$\mathcal{K}(\mathbf{f}) = \sum_{i=1}^{K} \frac{\mathbf{e}_i^T \left(H\mathbf{f} + b\,1 - \mathbf{g}\right) \mathbf{e}_i^T H\mathbf{f}}{\mathbf{e}_i^T (H\mathbf{f} + b\mathbf{1})} H^+ \mathbf{e}_i,$$

and $\mathbf{e}_i$ is the i-th canonical basis unit vector. Here $H^+ = (H^T H)^{-1} H^T$, $\mathbf{f}_G = H^+(\mathbf{g} - b\mathbf{1})$ and $H = [\mathbf{h}_1, \mathbf{h}_2, \cdots, \mathbf{h}_P] \in \mathbb{R}^{K \times P}$, is a system PSF matrix based on the estimated 3D locations .

Our Overall Process for 3D Point Source Localizations

1. Solve the minimization problem, KL-NC, using iteratively reweighted ℓ_1 algorithm;
2. Post Processing for removing false positives, using a centroid method;
3. Estimate the flux values of the point sources, using a fixed point iterative scheme.

Experimental Setup for Poisson Noise Case

- Consider different density cases:the number of point sources simulated in one image plane is 5, 10, 15, 30 and 40,respectively
- Randomly generate 50 different distributions of point sources for each case
- The number of photons emitted by each point source follows a Poisson distribution with mean of 2000 photons
- Fixed background $b = 5$
- Evaluation criteria: Recall rate & Precision rate

Localization for Low Density Case

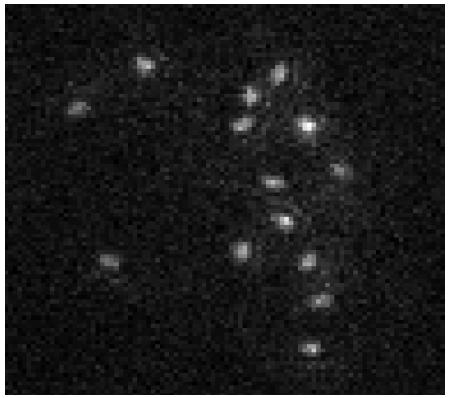

(a) Observed image

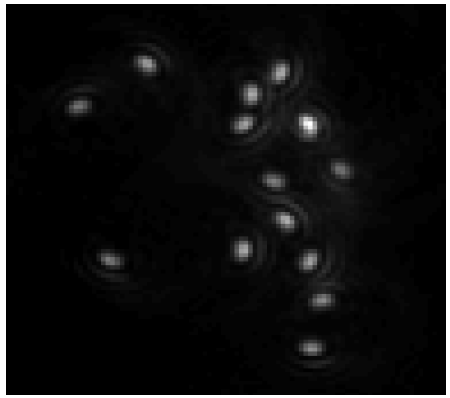

(b) Original image

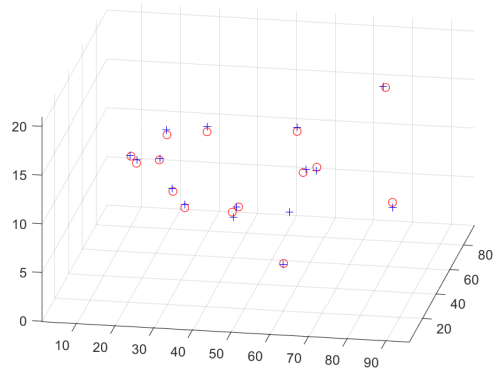

(c) Ground truth "o", estimate "+"

Localization for Higher Density Case with Overlaps

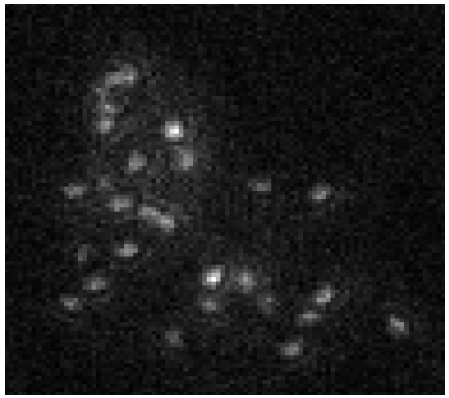

(c) Observed image

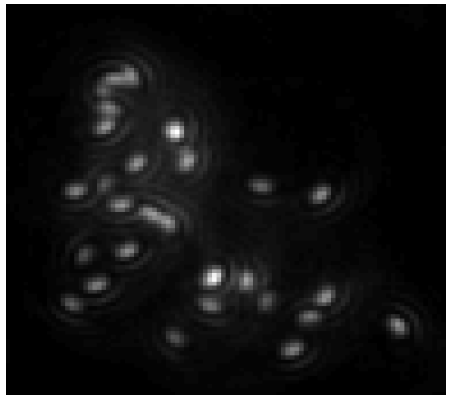

(d) Original image

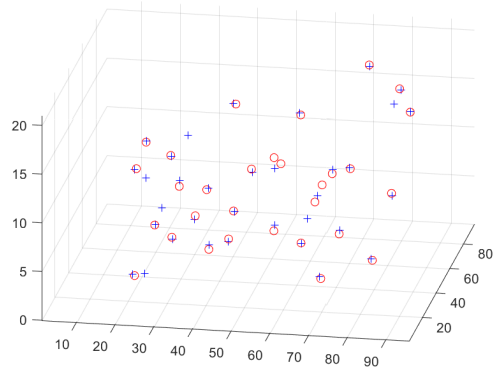

(c) Ground truth "o", estimate "+"

Comparison in Other Algorithms

Table: Comparison of KL-NC with KL-ℓ_1, ℓ_2-ℓ_1 and ℓ_2-NC. All the results are **after performing post-processing**.

	ℓ_2-ℓ_1		ℓ_2-NC		KL-ℓ_1		KL-NC	
No.	Recall	Prec.	Recall	Prec.	Recall	Prec.	Recall	Prec.
5	**100.00%**	68.41%	97.20%	87.95%	98.53%	58.67%	**100.00%**	**93.71%**
10	99.60%	56.54%	94.40%	83.33%	99.40%	65.33%	**100.00%**	**92.83%**
15	**99.20%**	54.20%	93.33%	83.45%	98.53%	58.67%	98.80%	**87.22%**
20	97.70%	56.03%	93.60%	78.89%	98.10%	57.76%	**98.60%**	**85.29%**
30	**95.67%**	54.16%	89.73%	74.63%	95.33%	54.54%	94.47%	**79.93%**
40	95.25%	49.32%	82.45%	51.63%	93.60%	53.87%	**95.40%**	**69.22%**

- Recall rate: $\dfrac{\textbf{Number of identified true positive emitters}}{\textbf{Number of all true emitters}}$
- Precision rate: $\dfrac{\textbf{Number of identified true positive emitters}}{\textbf{Number of all emitters identified by algorithm}}$

Estimation of Flux

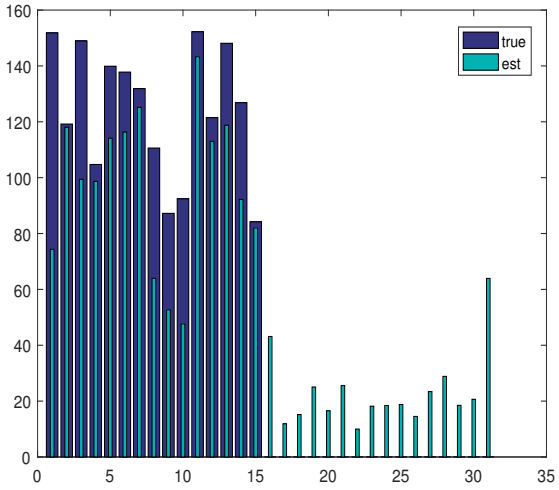

KL-ℓ_1

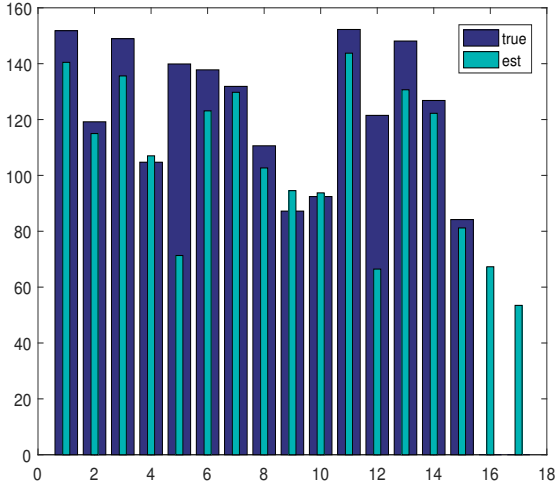

ℓ_2-NC

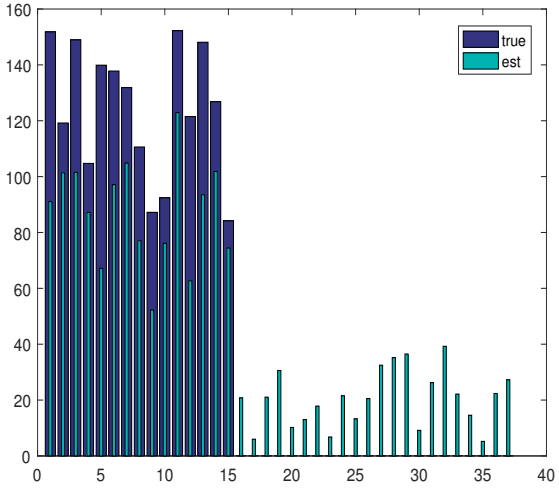

ℓ_2-ℓ_1

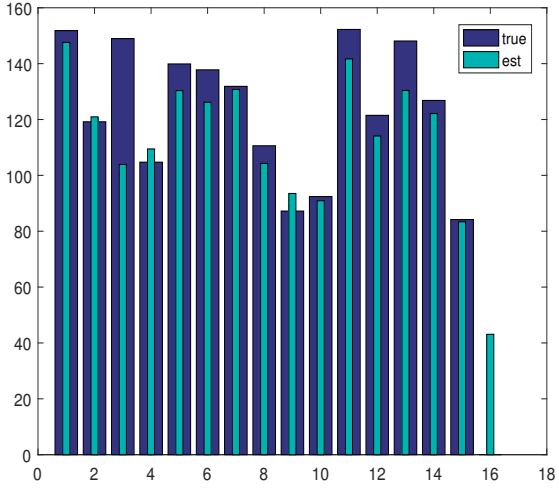

KL-NC

Limited-angle CT reconstruction via L_1/L_2 minimization

Background

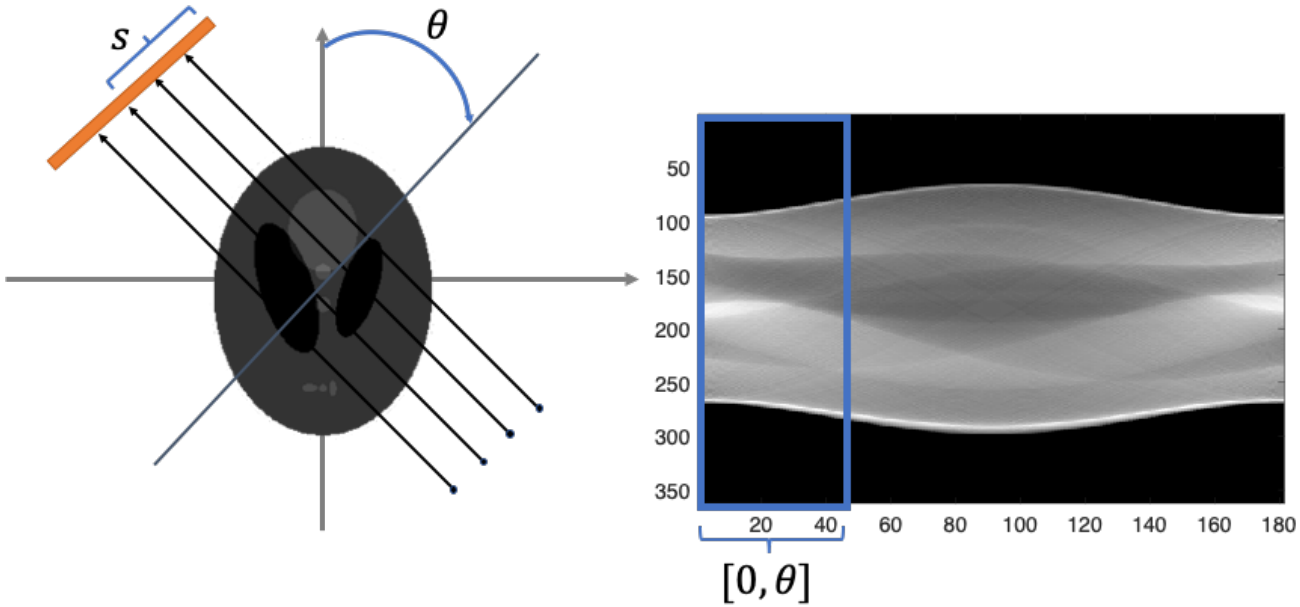

Limited angle scanning is due to

- low radiation exposure (3D mamography)
- short exposure time (motion reduction)
- engine exam
- ...

Mathematical model

- Forward physics model: Radon tranform

$$f(s,\theta) \approx \int_{(x,y)\in l(s,\theta)} u(x,y)dxdy$$

- Discretization:
  $Au = f$ (noiseless case)
  $Au + n = f$ (noisy case)
- Optimization model:
  $\min_{u\in\mathbb{R}^{n\times m}} \mathcal{R}(\nabla u) \quad \text{s.t.} \quad Au = f$, (noiseless case)
  $\min_{u\in\mathbb{R}^{n\times m}} \mathcal{R}(\nabla u) + \frac{1}{2}\|Au - f\|_2^2$, (noisy case)
- Proposed approximate metric: $\mathcal{R}(\mathbf{x}) = \frac{\|\mathbf{x}\|_1}{\|\mathbf{x}\|_2}$

Advantages of L_1/L_2

- Parameter free, unlike L_p, Transformed L_1, SCAD/MCP.
- Scale invariant (same as L_0)

$$\frac{\|\alpha \mathbf{x}\|_1}{\|\alpha \mathbf{x}\|_2} = \frac{|\alpha| \|\mathbf{x}\|_1}{|\alpha| \|\mathbf{x}\|_2} = \frac{\|\mathbf{x}\|_1}{\|\mathbf{x}\|_2}, \quad \forall \alpha \neq 0, \mathbf{x} \neq \mathbf{0}.$$

- Empirically shown to work well for high dynamic range signals, i.e., $\frac{\max\{|\mathbf{x}_S|\}}{\min\{|\mathbf{x}_S|\}}$ is large, where S is the support.
- Theoretical guarantee: under a null space property (NSP) type of condition, any sparse solution of $A\mathbf{x} = \mathbf{b}$ ($\mathbf{b} \neq \mathbf{0}$) is a local minimum for L_1/L_2 in the feasible space of $A\mathbf{x} = \mathbf{b}$.

SISC 2019 and TSP 2020.

L_1/L_2 on signal processing

Relationship with L_1-L_2

Define

$$\begin{aligned} \alpha^* &:= \min_{\mathbf{x}\in\mathbb{R}^n} \left\{ \frac{\|\mathbf{x}\|_1}{\|\mathbf{x}\|_2} \,\middle|\, A\mathbf{x} = \mathbf{b} \right\}, \\ T_\alpha &:= \min_{x\in\mathbb{R}^n} \left\{ \|\mathbf{x}\|_1 - \alpha\|\mathbf{x}\|_2 \,\middle|\, A\mathbf{x} = \mathbf{b} \right\}, \end{aligned}$$

then we have

$$\begin{cases} \alpha^* \in [1,\ \alpha] & \text{if } T_\alpha < 0 \\ \alpha^* \in [\alpha,\ \sqrt{n}] & \text{if } T_\alpha > 0 \\ \alpha^* = \alpha & \text{if } T_\alpha = 0. \end{cases}$$

Algorithm development — Speed-up by adaptive method 1

BS is computationally expensive, considering that L_1-αL_2 minimization is conducted for multiple times.

To speed up, we propose two variant of L_1/L_2-BS, one of which involves two simple steps:

$$\begin{aligned} \mathbf{x}^{(k+1)} &= \arg\min_{\mathbf{x}} \left\{ \|\mathbf{x}\|_1 - \left\langle \mathbf{x}, \frac{\alpha^{(k)}\mathbf{x}^{(k)}}{\|\mathbf{x}^{(k)}\|_2} \right\rangle \text{ s.t. } A\mathbf{x} = \mathbf{b} \right\} \\ \alpha^{(k+1)} &= \|\mathbf{x}^{(k+1)}\|_1 / \|\mathbf{x}^{(k+1)}\|_2. \end{aligned}$$

This algorithm is referred to as L_1/L_2-A1.

Algorithm development — Speed-up by adaptive method 2

BS is computationally expensive, considering that $L_1 - \alpha L_2$ minimization is conducted for multiple times.

To speed up, we propose a variant of L_1/L_2-BS, which involves two simple steps:

$$\begin{aligned}
\mathbf{x}^{(t+1)} &= \arg\min_{\mathbf{x}} \left\{ \|\mathbf{x}\|_1 - \left\langle \mathbf{x}, \frac{\alpha^{(t)}\mathbf{x}^{(t)}}{\|\mathbf{x}^{(t)}\|_2} \right\rangle + \frac{\beta}{2}\|\mathbf{x} - \mathbf{x}^{(t)}\|_2^2 \text{ s.t. } A\mathbf{x} = \mathbf{b} \right\} \\
\alpha^{(t+1)} &= \|\mathbf{x}^{(t+1)}\|_1 / \|\mathbf{x}^{(t+1)}\|_2.
\end{aligned}$$

This algorithm is referred to as L_1/L_2-A2.

Connections to generalized inverse power methods

- Inverse power: minimize Rayleigh quotient $q(x) = \frac{\langle \mathbf{x}, B\mathbf{x} \rangle}{\|\mathbf{x}\|^2}$ by iteratively solving

$$\mathbf{x}^{(k+1)} = \arg\min_{\mathbf{x}} \left\{ \frac{1}{2} \langle \mathbf{x}, B\mathbf{x} \rangle - \langle \mathbf{x}^{(k)}, \mathbf{x} \rangle \right\}$$

- Generalized inverse power[1] : $q(x) = \frac{r(\mathbf{x})}{s(\mathbf{x})}$ via

$$\mathbf{x}^{(k+1)} = \arg\min_{\mathbf{x}} \left\{ r(\mathbf{x}) - \alpha^{(k)} \langle \nabla s(\mathbf{x}^{(k)}), \mathbf{x} \rangle \right\}$$

- L_1/L_2-A1 is the generalized inverse power when $r(\mathbf{x}) = g(\mathbf{x}), s(\mathbf{x}) = \|\mathbf{x}\|_2$.
- L_1/L_2-A2 is the modified generalized inverse power[2]

[1] Hein & Büler, NIPS (2010)
[2] Bresson, et al. NIPS (2012)

Connections to gradient-based methods

- Equivalent form on the KKT conditions of L_1/L_2 model:

$$\begin{cases} 0 \in \partial\|\mathbf{x}^*\|_1 - \frac{\|\mathbf{x}^*\|_1}{\|\mathbf{x}^*\|_2}\frac{\mathbf{x}^*}{\|\mathbf{x}^*\|_2} + A^T\hat{\mathbf{s}} \\ 0 = A\mathbf{x}^* - \mathbf{b} \end{cases}$$

  where $\hat{\mathbf{s}} = \|\mathbf{x}^*\|_2\mathbf{s}$

- This is also an optimality condition to

$$\min_{\mathbf{x}} g(\mathbf{x}) + w(\mathbf{x}), \tag{2}$$

  where $\nabla w(\mathbf{x}) = -\frac{\|\mathbf{x}\|_1}{\|\mathbf{x}\|_2}\frac{\mathbf{x}}{\|\mathbf{x}\|_2}$

- L_1/L_2-A1 is a generalized conditional gradient method[3] on (2)
- L_1/L_2-A2 is a proximal gradient method on (2).

[3] Bredies, et al, COA (2009)

Convergence analysis

Theorem

Given a sequence $\{\mathbf{x}^{(k)}, \alpha^{(k)}\}$ *generated by* L_1/L_2*-A1. If* $\{\mathbf{x}^{(k)}\}$ *is bounded, it has a convergent subsequence.*

Theorem

Given a sequence $\{\mathbf{x}^{(k)}, \alpha^{(k)}\}$ *generated by* L_1/L_2*-A2. If* $\{\mathbf{x}^{(k)}\}$ *is bounded, there exists a subsequence, denoted by* $\{\mathbf{x}^{(k_i)}\}$*, that converges to a critical point.*

L_1/L_2 on the gradient

$$(L_1/L_2\text{-con}) \qquad \min_u \frac{\|\nabla u\|_1}{\|\nabla u\|_2} \quad \text{s.t.} \;\; Au = f.$$

We introduce $\mathbf{d}, \mathbf{h}$ to be equal to ∇u, thus leading to

$$\min_{u,\mathbf{d},\mathbf{h}} \frac{\|\mathbf{d}\|_1}{\|\mathbf{h}\|_2} \quad \text{s.t.} \;\; Au = f, \;\; \mathbf{d} = \nabla u, \;\; \mathbf{h} = \nabla u.$$

The augmented Lagrangian is expressed as

$$\begin{aligned}\mathcal{L}(u, \mathbf{d}, \mathbf{h}; w, \mathbf{b}_1, \mathbf{b}_2) = \frac{\|\mathbf{d}\|_1}{\|\mathbf{h}\|_2} &+ \langle \lambda w, f - Au \rangle + \frac{\lambda}{2}\|Au - f\|_2^2 \\ &+ \langle \rho_1 \mathbf{b}_1, \nabla u - \mathbf{d} \rangle + \frac{\rho_1}{2}\|\mathbf{d} - \nabla u\|_2^2 \\ &+ \langle \rho_2 \mathbf{b}_2, \nabla u - \mathbf{h} \rangle + \frac{\rho_2}{2}\|\mathbf{h} - \nabla u\|_2^2.\end{aligned}$$

SISC 2019.

Different splitting

The L_1/L_2-con model is equivalent to

$$\min_{u,\mathbf{h}} \frac{\|\nabla u\|_1}{\|\mathbf{h}\|_2} + \Pi_{Au=f}(u) \quad \text{s.t.} \quad \mathbf{h} = \nabla u,$$

where $\Pi_S(t)$ is an indicator function enforcing t into the feasible set S, i.e.,

$$\Pi_S(t) = \begin{cases} 0 & \text{if } t \in S \\ +\infty & \text{otherwise.} \end{cases}$$

The augmented Lagrangian function is given by

$$\mathcal{L}_{\text{con}}(u, \mathbf{h}; \mathbf{b}_2) = \frac{\|\nabla u\|_1}{\|\mathbf{h}\|_2} + \Pi_{Au=f}(u) + \langle \rho_2 \mathbf{b}_2, \nabla u - \mathbf{h} \rangle + \frac{\rho_2}{2} \|\mathbf{h} - \nabla u\|_2^2.$$

arXiv:2006.00601.

ADMM iterates as follows,

$$\begin{cases} u^{(k+1)} = \arg\min_u \mathcal{L}_{\text{con}}(u, \mathbf{h}^{(k)}; \mathbf{b}_2^{(k)}) \\ \mathbf{h}^{(k+1)} = \arg\min_{\mathbf{h}} \mathcal{L}_{\text{con}}(u^{(k+1)}, \mathbf{h}; \mathbf{b}_2^{(k)}) \\ \mathbf{b}_2^{(k+1)} = \mathbf{b}_2^{(k)} + \nabla u^{(k+1)} - \mathbf{h}^{(k+1)}. \end{cases}$$

The u-subproblem can be expressed as

$$u^{(k+1)} = \arg\min_u \frac{\|\nabla u\|_1}{\|\mathbf{h}^{(k)}\|_2} + \frac{\rho_2}{2}\|\mathbf{h}^{(k)} - \nabla u - \mathbf{b}_2^{(k)}\|_2^2 \quad \text{s.t.} \quad Au = f.$$

Convergence analysis

Theorem (convergence of L_1/L_2-box)

Under the Assumptions A1, A3, and a sufficiently large ρ_2, the sequence $\{u^{(k)}, \mathbf{h}^{(k)}\}$ generated by the splitting scheme of L_1/L_2-box always has a subsequence convergent to a critical point of L_1/L_2-box.

Theorem (convergence of inexact scheme in L_1/L_2-box)

Under the Assumptions A1-A3 and a sufficiently large ρ_2, one can solve the u-subproblem within an error tolerance ε_k and feasible set, i.e., $\|\tilde{u}^{(k+1)} - u^{(k+1)}\|_2^2 \leq \varepsilon_k$ and $\tilde{u}^{(k+1)} \in [c, d]$. If $\sum_k \varepsilon_k < +\infty$, then the resulting sequence $\{\tilde{u}^{(k)}, \mathbf{h}^{(k)}\}$ has a subsequence convergent to a critical point of L_1/L_2-box.

Standard phantoms

We discretize both phantoms at a resolution of 256×256. The forward operator A is generated with a parallel beam geometry sampled at $\theta_{\text{Max}}/30$ over a range of θ_{Max}, resulting in a sub-sampled data of size 362×31. The simulation process is available in the IR and AIR toolbox

Figure: Ground truth of Shepp-Logan (SL) phantom, FORBILD (FB) head phantom and real data walnut with the gray scale window of $[0,\ 1]$, $[1.03,\ 1.10]$, and $[0,\ 1.5]$, respectively.

Comparison

Table: CT reconstruction of the parallel beam in the SL phantom by SART, L_1, L_1-L_2, and L_1/L_2.

noise	range	SART		L_1		L_1-L_2		L_1/L_2	
		SSIM	RMSE	SSIM	RMSE	SSIM	RMSE	SSIM	RMSE
0.5%	90°	0.56	13.81%	0.88	7.52%	0.78	8.75%	0.96	1.74%
	150°	0.58	10.57%	0.98	3.75%	0.88	3.43%	0.98	1.05%
0.1%	90°	0.58	13.68%	0.96	4.12%	0.88	7.16%	1.00	0.29%
	150°	0.60	10.37%	0.98	3.48%	0.99	0.76%	1.00	0.11%

SART: simultaneous algebraic reconstruction technique, 1984.

Synthetic data

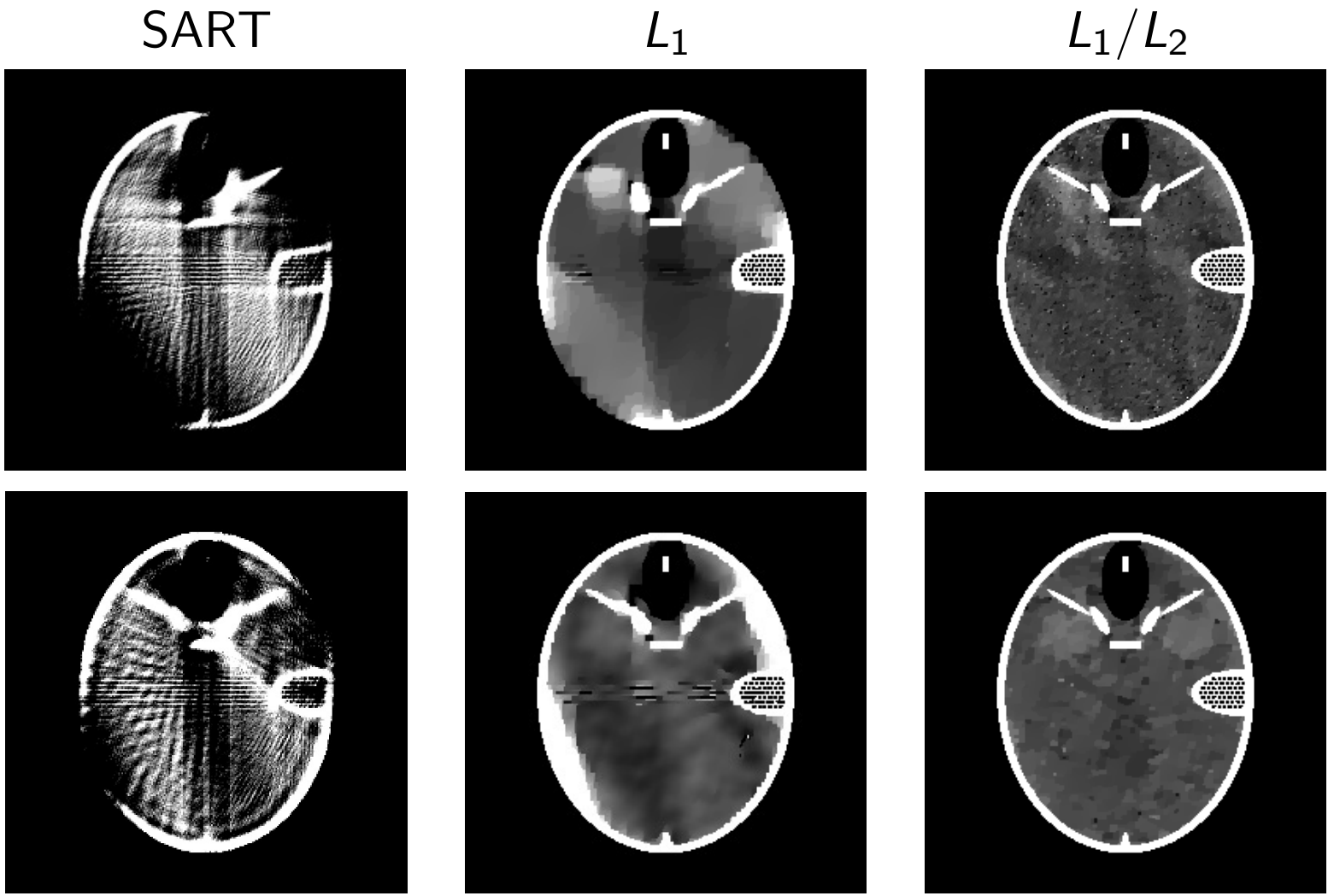

Figure: CT reconstruction from 90° (top) and 135° (bottom) projection range for the FB phantom with 0.1% noise.

Experimental data

SART

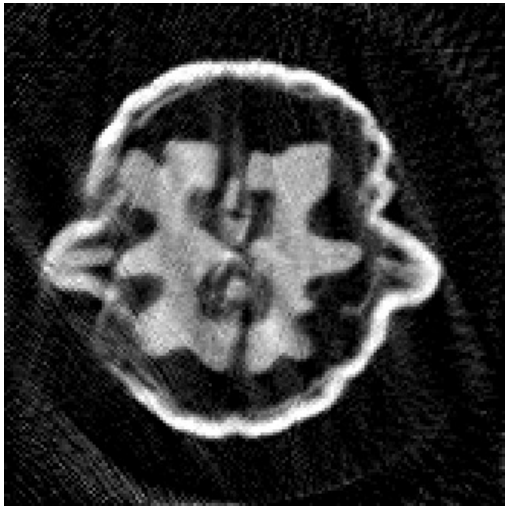

L_1

L_1-L_2

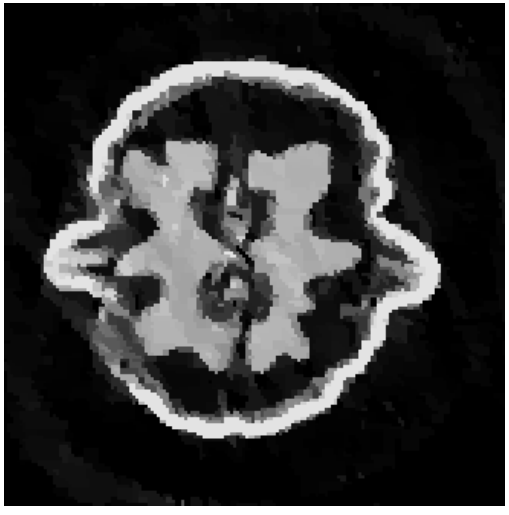

L_1/L_2

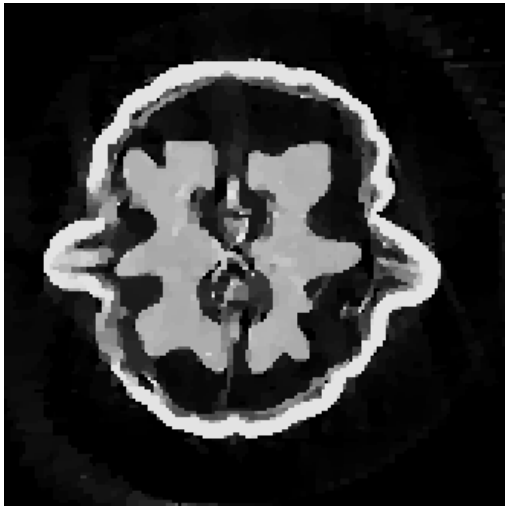

Conclusions

- PSF:
  - Develop novel nonconvex regularization method based on Kullback-Leibler Divergence (KL-NC)
  - Iterative scheme for estimating flux
- Limited-angle CT:
  - Compressed sensing approach to handle limited observed data issue
  - Explore the performance of L_1/L_2 from signal processing to medical imaging reconstruction

Stories still continue...(on-going projects at UCD)

1. Quantitative Susceptibility Mapping (QSM) in MRI (cooperated with Prof. Audrey Fan in Dept. BME)
2. Extension of L_1/L_2 (cooperated with Prof. Shiqian Ma in Dept. Math)

Thank you